Silicon Photonic Integrated Circuits under Process Variations

Mahdi Nikdast[1,2*], Gabriela Nicolescu[1], Jelena Trajkovic[3], Odile Liboiron-Ladouceur[2]
[1]*CE Dep., Polytechnique Montreal, Montreal, Canada* [2]*ECE Dep., McGill University, Montreal, Canada*
[3]*ECE Dep., Concordia University, Montreal, Canada*
mnikdast@ieee.org

Abstract: Developing a computationally efficient and accurate bottom-up method, we systematically study process variations in passive silicon photonic integrated circuits. Comparisons with numerical simulations indicate the high efficiency of our proposed method.

1. Introduction

Precise central wavelength matching among different devices in photonic integrated circuits (PICs) is of critical concern when employing WDM and using devices such as microresonators (MRs) and optical filters. Such devices, however, are susceptible to process variations, a.k.a. fabrication non-uniformity. As a result, the behavior of a fabricated photonic device is very often different from what has been expected during its design process. Understanding the fabrication variability is essential for developing strategies for the system implementation, and for determining the cost implications for some compensations strategies, such as thermal tuning.

The dominant variations in silicon photonics are those in the top silicon thickness and feature size [1,2]. Moreover, these variations differ from wafer to wafer as well as within a single PIC. For example, [3] demonstrated within-wafer variations of 10 nm in the top silicon thickness. When designing a single photonic device, one may consider several design parameter sweeps, while performing numerical simulations (e.g. FDTD), to learn about the variations in the device characteristics after its fabrication. Nevertheless, this technique is not applicable to large-scale systems consisting of hundreds and thousands of different photonic devices (e.g. inter- /intra-chip photonic interconnects) due to its enormous computation cost.

In this paper, we present a computationally efficient systematic bottom-up approach to study the impact of process variations on large-scale passive silicon photonic interconnects (SPIs). Considering detailed physical properties of photonic components, we first model process variations at the component level (i.e. waveguides), and then at the device level (i.e. photonic switches and filters). Compared with costly numerical simulations, we demonstrate that our proposed analyses can be applied to study random process variations in large-scale SPIs, while achieving a high accuracy and low computation cost. In the rest of this paper, we briefly go through the proposed component and device level analytical models. Moreover, we quantitatively simulate the proposed analytical models and also compare the results with those from the numerical simulations.

2. Theoretical Models

We start by analyzing the effective and group indices of strip waveguides, which can be altered by process variations. The fundamental TE mode is considered, while the analyses for the TM mode can be similarly developed. An extended version of the Marcatili's approach, which is applicable to high-index-contrast waveguides, is considered to characterize strip waveguides [4]. We improve this method by modeling the impact of process variations on the effective and group indices of waveguides. Our proposed improved Marcatili's method (IMM) approximates a 3D strip waveguide, shown in Fig. 1a, with a simplified 2D structure that is depicted in Fig. 1b. The core is from Si and its refractive index, n_{cr}, is modeled based on the Sellmeier equation to consider the impact of the material dispersion [5]. The homogeneous surrounding regions II, III, IV and V are all from SiO_2 and have equal refractive indices of 1.444.

Considering Fig. 1b, we can derive the wave equations for region I [4]. Accordingly, the propagation constant that includes the variations in the silicon thickness and waveguide width can be defined as:

$$\beta(T_s,W_s,\lambda) = k_0 n_{eff}(T_s,W_s,\lambda) = \sqrt{n_{cr}(\lambda)^2 k_0^2 - k_x(T_s,W_s,\lambda)^2 - k_y(T_s,W_s,\lambda)^2}, \quad (1)$$

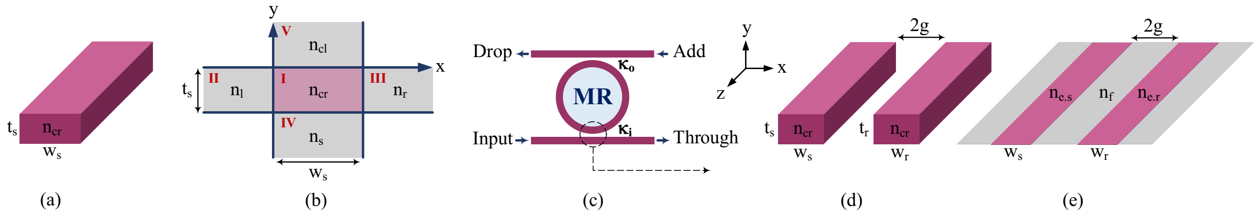

Fig. 1. (a) A 3D strip waveguide, (b) a 2D approximation of the strip waveguide based on the IMM method, (c) an MR-based add-drop filter, (d) a 3D directional coupler model for the coupling region in add-drop filters, and (e) a 2D approximation of the coupler.

in which T_s and W_s are the thickness and width of the waveguide under variations, and they are respectively equal to $t_s \pm \rho_t$ and $w_s \pm \rho_w$, where ρ_t and ρ_w are defined as the variations in the silicon thickness and waveguide width, respectively. k_0 is the free-space wavenumber. $n_{cr}(\lambda)$ is the refractive index of the waveguide core based on the Sellmeier equation. Also, n_{eff} is the effective index, while k_x and k_y are the spatial frequencies that can be calculated using the following eigenvalue equations obtained by respecting the boundary conditions at the I-IV-V interfaces and I-II-III interfaces (see Fig. 1b):

$$tan\left[k_x(T_s,W_s,\lambda)W_s\right] = \frac{n_{cr}(\lambda)^2 k_x(T_s,W_s,\lambda)\left(n_r^2\gamma_l + n_l^2\gamma_r\right)}{n_l^2 n_r^2 k_x(T_s,W_s,\lambda)^2 - n_{cr}(\lambda)^4\gamma_l\gamma_r}, \qquad tan\left[k_y(T_s,W_s,\lambda)T_s\right] = \frac{k_y(T_s,W_s,\lambda)\left(\gamma_s+\gamma_{cl}\right)}{k_y(T_s,W_s,\lambda)^2 - \gamma_s\gamma_{cl}}, \quad (2)$$

where $\gamma_{l/r}^2 = \left(n_{cr}^2(\lambda) - n_{l/r}^2\right)k_0^2 - k_x^2$, and $\gamma_{s/cl}^2 = \left(n_{cr}^2(\lambda) - n_{s/cl}^2\right)k_0^2 - k_y^2$. Employing (1) and (2), we can calculate the impact of silicon thickness and waveguide width variations on the propagation constant, and hence the effective index of a strip waveguide. Moreover, the group index can be calculated as $n_g(T_s,W_s,\lambda) = n_{eff}(T_s,W_s,\lambda) - \lambda\frac{dn_{eff}(T_s,W_s,\lambda)}{d\lambda}$.

Fig. 1c depicts an MR-based add-drop filter. Analyzing the resonance wavelength shift in an MR, we need to take into account the impact of waveguide dispersion ($\frac{\partial n_{eff}}{\partial\lambda} \neq 0$). Considering the first order approximation of the waveguide dispersion and group index calculation, the resonance wavelength shift is modeled as $\Delta\lambda_{res} = \frac{\Delta_{\rho_{t/w}} n_{eff}.\lambda_{res}^0}{n_g(t_s,w_s,\lambda_{res}^0)}$. In this equation, $\Delta_{\rho_{t/w}} n_{eff}$ includes the effective index alterations due to the silicon thickness or waveguide width variations, λ_{res} is the primary resonance wavelength of the MR with no variations, and $\Delta\lambda_{res}$ is the resonance wavelength shift [6].

Considering Fig. 1c, we assume that the input and drop waveguides are symmetrically coupled to the MR, i.e. $\kappa_i = \kappa_o$, and the coupler is lossless. Also, we assume that $W_r = W_s$ and $T_r = T_s$, i.e. while $w_r = w_s$ and $t_r = t_s$, the variations in the waveguide and MR are also the same. The coupling region in Fig. 1c is modeled in Fig. 1d as a directional coupler. The cross-over coupling coefficients and length are analyzed based on the supermode theory [7]. Using the difference between the effective indicies of the first two symmetric and antisymmetric supermodes of the coupler, $\Delta n_{eff}(T_r,W_r,\lambda)$, the cross-over coupling coefficients can be found as $\kappa_{i/o}(T_r,W_r,\lambda) = \left|sin\left(\frac{\Delta n_{eff}(T_r,W_r,\lambda)\pi}{\lambda}L\right)\right|$, in which L is the length of the coupler. Moreover, the cross-over length can be calculated as $L_c(T_r,W_r,\lambda) = \frac{\lambda}{2\Delta n_{eff}(T_r,W_r,\lambda)}$. The coupler can be approximated with the two strip waveguides indicated in Fig. 1e, in which $n_{e.s}(T_s,W_s,\lambda) = n_{e.r}(T_r,W_r,\lambda)$ is the effective index of the slab waveguide in the y direction in Fig. 1d, and it can be calculated based on the proposed IMM method. Also, $n_f = 1.444$. Considering the five-layer slab waveguide shown in Fig. 1e, the effective indices of the symmetric and antisymmetric supermodes can be calculated using:

$$tan(2N_1) = \frac{N_1N_2\left(1+tanh(2N_2g/W_r)\right)}{N_1^2 - N_2^2 tanh(2N_2g/W_r)}, \qquad N_1 = k_0\frac{W_r}{2}\sqrt{n_{e.r}^2 - (\beta/k_0)^2}, \qquad N_2 = k_0\frac{W_r}{2}\sqrt{(\beta/k_0)^2 - n_f^2}, \quad (3)$$

in which for the antisymmetric mode *tanh* should be replaced by *coth* [8].

3. Results and Discussion

We implemented the proposed analytical models in MATLAB. The numerical simulation was performed in MODE, a commercial-grade simulator eigenmode solver and propagator [9]. We consider a variation range of $\rho_{t/w} \in [-30,30]$ nm. Fig. 2 indicates the effective and group indices changes due to the variations in the silicon thickness and waveguide width in a strip waveguide. As the figure indicates, the proposed IMM demonstrates a very good approximation with an error rate of only 1%. Fig. 3(a) depicts the resonance wavelength shift in an MR-based add-drop filter, which

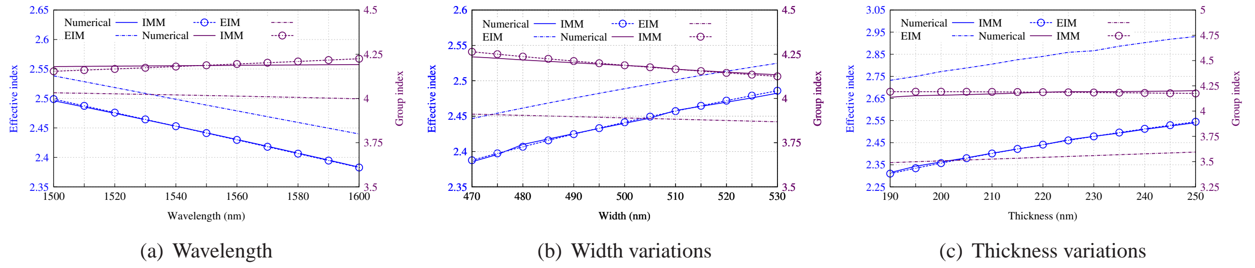

(a) Wavelength (b) Width variations (c) Thickness variations

Fig. 2. Effective and group indices of a strip waveguide under (a) different wavelengths, (b) width variations, and (c) thickness variations. We consider w_s=500 nm, t_s=220 nm, and the central wavelength, λ, equals 1550 nm. Results are compared and indicated for the proposed IMM method, the effective index method (EIM), and the numerical simulation performed in MODE.

is independent of the MR radius, under process variations. As can be seen, the resonance wavelength shift is considerable especially when the silicon thickness varies ($\approx$90 nm shift in total). Similar results have been experimentally demonstrated in other work [1–3]. Fig. 3(b) shows the cross-over length variations, while the cross-over coupling coefficients, when $L=$10 μm, is indicated in Fig. 3(c). As the width of the waveguides increases, the gap (2g in Fig. 1e) decreases. As a result, L_c decreases when the waveguides get wider. Under thickness variations, however, the gap is fixed, and the changes in the effective indices vary L_c. In both Figs. 2 and 3, the proposed method computed the results in a few seconds, while the numerical method took more than an hour to complete (>100× improvement). In practice, $\rho_{t/w} \in [-10, 10]$ nm for within-die variations [1, 3], and the proposed method is highly accurate in this range.

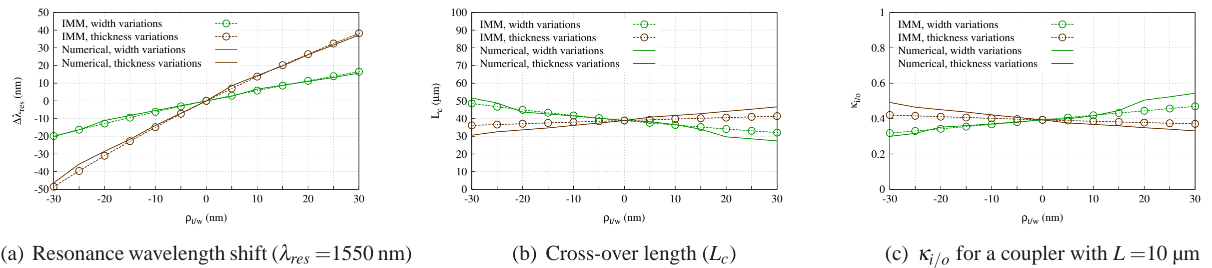

(a) Resonance wavelength shift ($\lambda_{res}=$1550 nm) (b) Cross-over length (L_c) (c) $\kappa_{i/o}$ for a coupler with $L=$10 μm

Fig. 3. (a) The resonance wavelength shift, (b) cross-over length, and (c) cross-over coupling coefficients under process variations ($w_s = w_r =$500 nm, $t_s = t_r =$220 nm, and 2g=200 nm).

In conclusion, we propose a simply implementable and efficient method to study process variations in large-scale passive silicon photonic interconnects. Comparisons with numerical simulations indicate the accuracy of our developed models, while the computation time is substantially shorter. The low computation cost of the proposed method enables its application to large-scale photonic interconnects, in which the employment of numerical simulations (e.g. FDTD) is not feasible.

We acknowledge ReSMiQ, SiEPIC, and NSERC for funding this project.

References

1. L. Chrostowski, *et. al.*, "Impact of fabrication non-uniformity on chip-scale silicon photonic integrated circuits," *OFC*, 2014.
2. R. G. Beausoleil, *et. al.*, "Devices and architectures for large-scale integrated silicon photonics circuits ," *Proc. of SPIE*, 7942, 2011.
3. W. Zortman, *et. al.*, "Silicon photonics manufacturing," Opt. Express , 18, pp. 23598-23607, 2010.
4. W. J. Westerveld, *et. al.*, "Extension of marcatili's analytical approach for rectangular silicon optical waveguides," J. of L. Tech. , 30, pp. 2388-2401, 2012.
5. D. F. Edwards, *et. al.*, "Infrared refractive index of silicon," Applied Optics , 19, pp. 4130-4131, 1980.
6. W. Bogaerts, *et. al.*, "Silicon Microring Resonators," Laser Photonics Reviews , 6, pp. 47-73, 2012.
7. L. Chrostowsk, *et. al*, Silicon Photonics Design From Devices to Systems. Cambridge U. P., 2015.
8. K. S. Chiang, Integrated optic waveguides, Enc. of Electrical and Electronics Eng., J. Webster, 2007.
9. Lumerical Solutions, Inc. http://www.lumerical.com/tcad-products/mode/.

160.39.37.59 {ts '2018-03-30 18:19:20'}